Research on Oil-CO_2-Water Relative Permeability of the Low Permeability Reservoir Based on History Matching

Fengli Zhang, Tianjin Branch of CNOOC, Tianjin, China; **Wenfeng Lv**, Research Institute of Petroleum Exploration and Development (RIPED), PetroChina, Beijing, China; **Yongyi Zhou**, North China Petroleum Bureau, Sinopec, Zhengzhou, China; **Bochao Qu**,**Yawen He**, **Xinle Ma**, **Weidong Tian**, and **Zhenzhen Dong***, Xi'an Shiyou University, Xi'an, China

Abstract

Accurate prediction of the relative permeability curve provides the basis for study of the CO_2 flooding effects (such as swept volume and oil displacement efficiency) and optimization of the CO_2 flooding plan. Considering that laboratory experiments are time-consuming and effort-consuming, and experimental results are easily affected by external factors, a method was proposed to calculate the relative permeability curve of the oil-CO_2-water multiphase fluid based on particle swarm optimization (PSO). The typical CO_2 flooding experiments in the low-permeability cores were performed, a multiphase flow numerical model was established in CMG-GEM, and 26 parameters of the model were optimized using the PSO method. The results of the model fitting are consistent with the results of the experiment, and the relative permeability of oil-CO_2 water, the capillary pressure of oil-water and the capillary pressure of gas-liquid of the low-permeability core were obtained. The validity of the model was verified in the research that the prediction from the numerical model is consistent with the laboratory experiment results. This study provides guidance for determining the oil-CO_2-water relative permeability of the low-permeability core.

Introduction

The relative permeability curve, a parameter reflecting the seepage law of multi-phase fluids in the porous media, is used to describe the movement of each fluid phase in the reservoir and predict the basic production index such as oil recovery rate, ultimate recovery factor, and water cut, and it is an important indicator in reservoir evaluation(Zhang et al. 2010). The relative permeability curve is of great significance to the study of fluid distribution in the process of CO_2 flooding, and it is used to understand the characteristics of both miscible and immiscible CO_2 flooding(Zhang et al. 2019). Therefore, accurate prediction of the relative permeability curve in CO_2 flooding provides the basis for the study of the swept volume, the oil displacement effect, fine reservoir description, and plan optimization in CO_2 flooding(Zhang et al. 2016).

Currently, the oil-water relative permeability curve is obtained through the steady-state method, the transient method, and the history matching method(Toth et al. 2002; Li et al. 2018; Li 1989; Eydinov et al. 2009).

DOI:10.14800/IOGR.1187
Received March 23, 2021; revised May 15, 2021; accepted June 18, 2021.
*Corresponding author: dongzz@xsyu.edu.cn

Typical CO_2 Flooding Experiment of Low-Permeability Cores

Experimental Materials and Fluids. The CO_2 flooding device in the low-permeability core is shown in **Figure 1**.

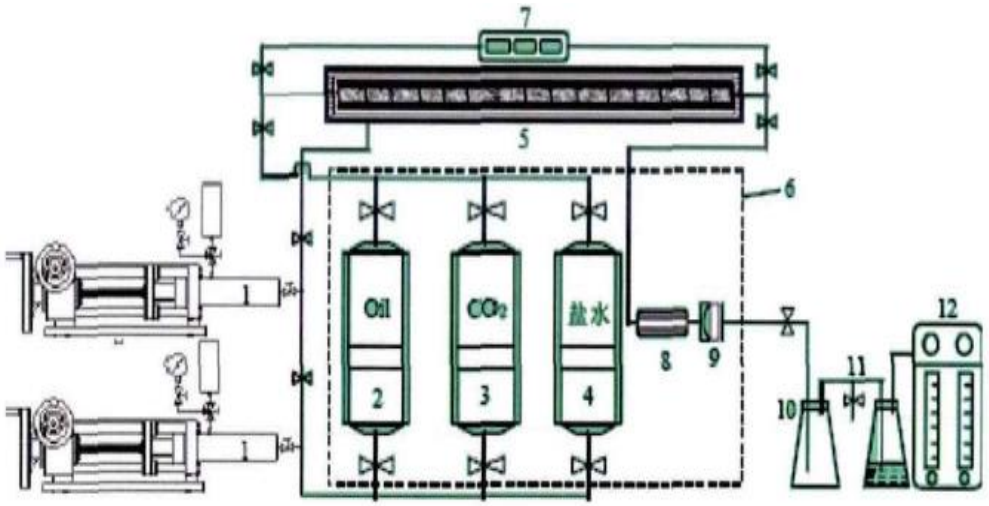

Figure 1—Device of displacement in the low-permeability core: 1.Displacement pump; 2.Oil vessel; 3.CO2 gas vessel; 4.Brine vessel; 5.Long core clamp; 6.Thermostat; 7.Pressure sensor; 8.Inspection window; 9.Pressure relief valve; 10.Separation bottle; 11.Sample tap; 12.Gasometer.

Constant composition expansion experiments of the oil from low- permeability reservoirs were carried out to obtain the in-place oil and its volume factor. The fluid model was established by dividing the pseudo-components through PVT fitting. The compositions of original components and pseudo-components are listed in **Table 1**.

Table 1—Pseudo-components of fluids in low-permeability reservoirs.

Original components	Mole compositions, mol%	Post-division components	Mole compositions, mol%
CO_2	0.113	CO_2	0.11
N_2	1.39	N_2 -CH_4	22.90
CH_4	21.533	C_2H-C_3H	5.26
C_2H_6	3.148	IC_4-C_6	1.76
C_3H_8	2.119	C_7-C_{11}	23.31
i-C_4H_{10}	0.348	C_{11}-C_{20}	23.31
n-C_4H_{10}	0.658	C_{21+}	23.31
i-C_5H_{12}	0.167		
n-C_5H_{12}	0.216		
C_6H_{14}	0.367		
C_{7+}	69.941		
Total	100		100

The fitting error of fluid viscosity and density with the pressure of the experiment is less than 5% (**Figures 2** and **3**).

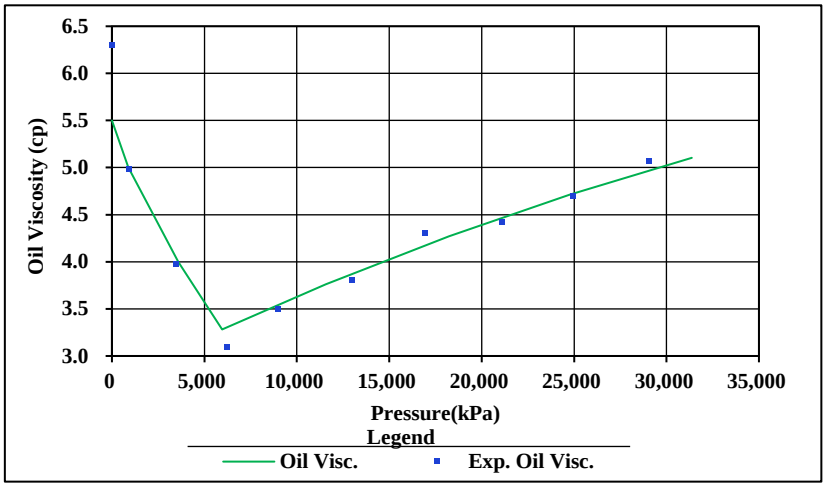

Figure 2—Fitting result of the oil viscosity at the formation temperature.

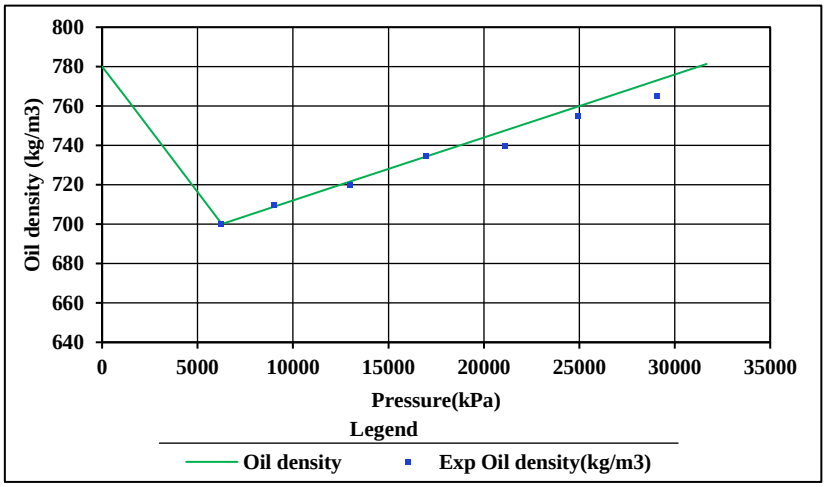

Figure 3—Fitting result of the oil density at the formation temperature.

Experimental Method. The experiments of water flooding in the cores under the formation state were performed. Water flooding continued until the water cut is above 98% and is stabilized for a period of time. Then, CO_2 flooding started and continued until the core is at the residual oil state. In the experiments, the displacement pressure and the oil, water and gas production were recorded at the designed time interval. The basic parameters of the displacement experiment of the cores from the low permeability reservoirs are listed in **Table 2**.

Table 2—Basic parameters and conditions of the displacement experiment of the cores from the low permeability reservoirs.

Parameters	Values
Experimental temperature (°C)	75.0
Experimental pressure (MPa)	17
Water injection rate (cm^3/min)	0.1
CO_2 injection rate (cm^3/min)	0.1
Air permeability (mD)	1.2
Porosity (%)	13.2
Irreducible water saturation (%)	35

Results. The experimental results are shown in **Figure 4**, which include gas-oil ratio, water cut, injection well bottom-hole pressure, and oil recover. In the water flooding period, the water cut increases to 98%, the gas-oil ratio is zero, and the recovery factor increases to 41%. During CO_2 flooding period, gas-oil ratio rises up quickly in the beginning and stabilizes around 14900 m^3/m^3, water cut drops dramatically and then increases to 80%, and the oil recovery increases from 41% to 89%.

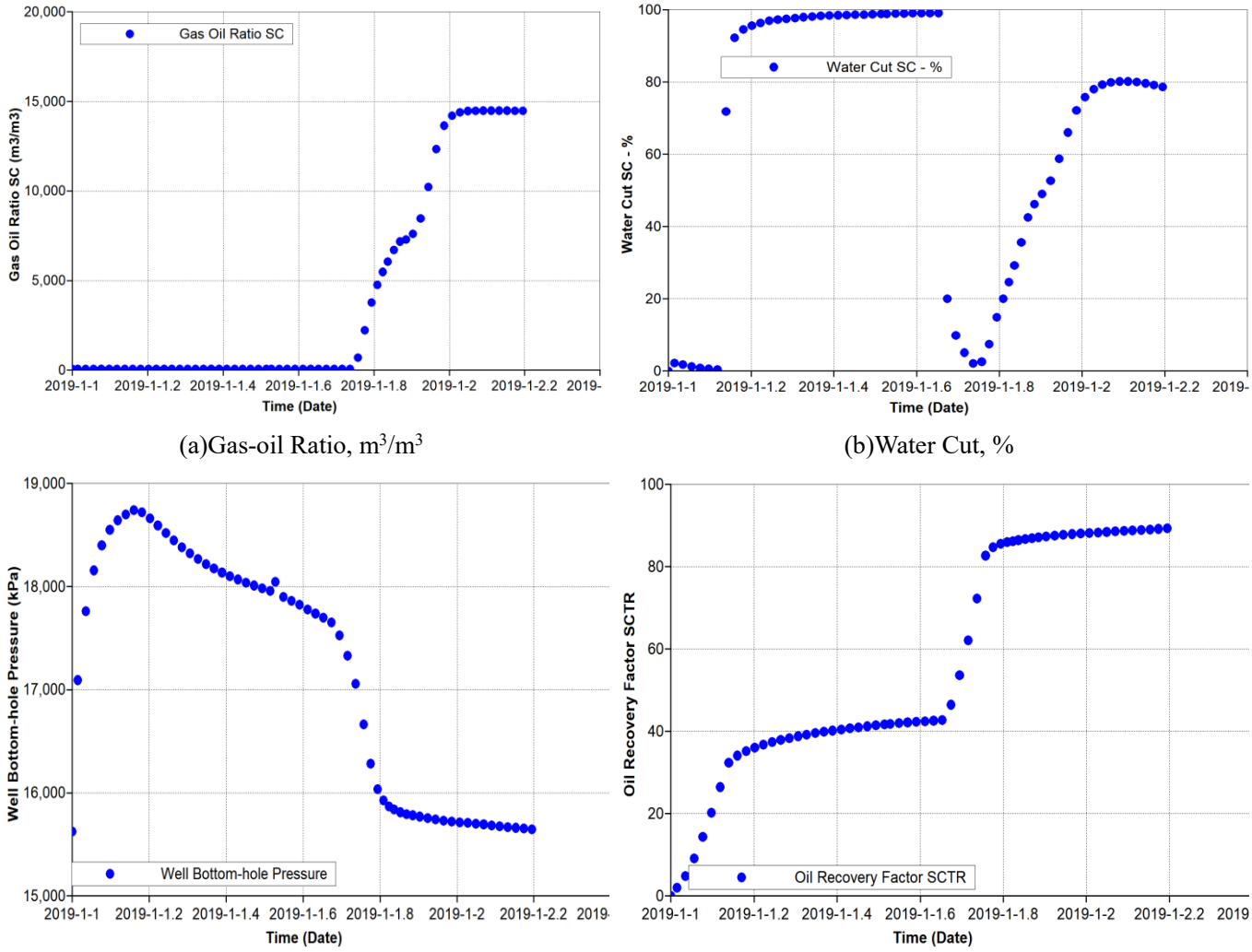

(a)Gas-oil Ratio, m^3/m^3 (b)Water Cut, %

(c) Injection Well Bottom-hole Pressure, kPa (d)Oil Recovery, %

Figure 4—Results of displacement experiment of the low-permeability cores.

Theoretical Model

Relative Permeability Curve Model of CO_2 Flooding. The compositional model in the commercial software CMG was used to simulate CO_2 flooding, and the Corey model of the relative permeability model in CMG was first proposed and has been widely adopted(CMG Manual 2015). The Corey model is expressed as follows.

Oil and water relative permeability

$$k_{rw} = k_{rwiro} \times \left(\frac{S_w - S_{wcrit}}{1 - S_{wcrit} - S_{oirw}}\right)^{n_w}, \quad \text{.....(1)}$$

$$k_{row} = k_{rocw} \times \left(\frac{S_o - S_{orw}}{1 - S_{wcon} - S_{orw}}\right)^{n_{ow}} \quad \text{.....(2)}$$

Gas and liquid relative permeability

$$k_{rog} = k_{rogcg} \times \left(\frac{S_l - S_{org} - S_{wcon}}{1 - S_{gcon} - S_{org} - S_{wcon}}\right)^{n_{og}} \quad \text{.....(3)}$$

$$k_{rg} = k_{rgcl} \times \left(\frac{S_g - S_{gcrit}}{1 - S_{gcrit} - S_{oirg} - S_{wcon}}\right)^{n_g} \quad \text{.....(4)}$$

The relationship between the capillary pressure and the saturation of core is expressed as follows.

Oil and water

$$p_{cow} = [p_{cow}(S_w = S_{wc_{on}}) - p_{cow}(S_w = 1 - S_{orw})] \times \left[\frac{(1 - S_{orw} - S_w)}{(1 - S_{wcon} - S_{orw})}\right]^{n_{ow}} + \boldsymbol{p_{cow}}(S_w = 1 - S_{orw}) \quad \text{.....(5)}$$

Gas and liquid

$$p_{cog} = \left[p_{cog}(S_l = S_{lcon}) - p_{cog}\left(S_l = 1 - S_{gcon}\right)\right] \times \left[\frac{(1 - S_{org} - S_g)}{(1 - S_{gcon} - S_{org})}\right]^{\boldsymbol{n_{og}}} + p_{cog}(S_w = 1 - S_{org}) \quad \text{.....(6)}$$

In the CMG-GEM module, the relative permeability curve is interpolated with the interfacial tension method. Fluids are considered immiscible when the interfacial tension is relatively large. The relative permeability curve and the capillary curve are assigned to both oil and gas. When the interfacial tension drops to the critical value, interpolation is performed with the formulas method to obtain the relative permeability curve and the capillary curve of oil and gas. The fluids are miscible when the interfacial tension is lower than the critical value. The relative permeability curves are selected according to the miscible modes.

The effect of interfacial tension on relative permeability is considered to obtain the linear functions of gas and oil saturation from gas and oil relative permeability curves when the fluid phases are miscible (the dual phase interfacial tension approaches 0). The corrected k_{ro} and k_{rg} are expressed with k_{rot} and k_{rgt} as follows.

$$k_{rot} = f * k_{ro} - (1 - f) * k_{ro} \frac{S_o}{(1 - S_w)}, \quad \text{.....(7)}$$

$$k_{rgt} = f * k_{rg} - (1 - f) * k_{rh} \frac{S_g}{1 - S_w}, \quad \text{.....(8)}$$

where,

$$k_{rh} = 0.5 * (k_{row}(S_w)) + k_{rg}(S_g = 1 - S_w), \quad \text{.....(9)}$$

$$f = \begin{cases} 1, if(\sigma > \sigma_0) \\ \left(\frac{\sigma}{\sigma_0}\right) \wedge eksig, otherwise \end{cases}, \quad \text{.....(10)}$$

$$\sigma^{\frac{1}{4}} = [P](\rho_L - \rho_g) \quad \text{.....(11)}$$

where $[P]$ is a temperature-independent parameter, which is estimated by molecular structure. When the interfacial tension is determined using this method, the unit of interfacial tension is dyn/cm and the unit of density is mol/cm^3.

When *eksig*>1 and $\sigma < \sigma_0$, the function is transformed into the linear function. When *eksig*<1, the transformation is delayed. When σ drops to a small part of σ_0, the function is transformed into the linear function. When *eksig*=1, the function is in a transition to an asymptotic linear function.

The effect of interfacial tension on the gas-oil capillary pressure causes the dual-phase pressure difference approach zero. The modified p_{cog} is expressed with p_{cogt} as,

$$p_{cogt} = \begin{cases} p_{cog}, & if\ \ \sigma > \sigma_0 \\ p_{cog} * \left(\frac{\sigma}{\sigma_0}\right)^{epsig}, & otherwise \end{cases} \quad \text{.....(12)}$$

Parameter Selection. In this paper, based on the known core data and by integrating **Eqs. 1** through **12**, the parameters listed in **Table 3** are selected to fit the data from the CO_2 flooding experiments.

Table 3—Model parameters and their value.

	Model parameters	parameters range
CO_2 Miscible interpolation parameters	eksig	0.01~1
	epsig	0.01-1
	σ_0	0.01~20
	sigms	0.0005-0.0015
Oil and water permeability parameters	SWCON(%)	0.46
	SWCRIT(%)	>0.46
	1-SORW(%)	0.5-0.9
	1-SOIRW(%)	>1-SORW
	KROWMAX	0.1-1
	KRWMAX	0.1-1
	NO	0.5-5
	NW	0.5-5
Gas and liquid permeability parameters	SOIRG(%)	0.05-0.3
	SORG(%)	>SOIRG
	SGCON(%)	0-0.1
	SGCRIT(%)	>SGCON
	KRGMAX	0.1-1
	KROGMAX	=KROWMAX
	NL	0.5-5
	NG	0.5-5
Capillary pressure parameters	PCOWMAX(kPa)	120-300
	PCOGMAX(kPa)	30-100
	PCOWMIN(kPa)	0-400
	PCOGMIN(kPa)	0-100
	NPOW	1-10
	NPGL	1-10

Particle Swarm Optimization (PSO) Algorithm. The parameters are optimized with the PSO method, where each particle has a memory to track the optimum iteration positions of the previous generation of particles. One position is found by the particle itself and is called the best position of the individual particle, and the other position is found by the entire particle group currently and is called the global best particle position. It is assumed that there are N particles in the D-dimensional search space, i.e., the population size of the particle swarm is N, where the position parameter of the i_{th} particle in the D-dimensional position is expressed as

$$x_i(k) = (x_{i1}(k), x_{i2}(k), \cdots, x_{iD}(k)) \quad \text{.....(13)}$$

The cost function of the optimization problem is used to judge whether the current position of the particle is superior to its history positions (Zhang 2017).The individual optimum position parameter (p_{best}) searched by the i_{th} particle is expressed as

$$p_{best} = (p_{i1}, p_{i2}, \cdots, p_{iD}) \quad (14)$$

The optimal position parameter (g_{best}) of the population searched by all particles is expressed as

$$g_{\text{best}} = (p_{g1}, p_{g2}, \cdots, p_{gD}) \quad (15)$$

The velocity is expressed as

$$v_i(k) = (v_{i1}(k), v_{i2}(k), \cdots, v_{iD}(k)) \quad (16)$$

The velocity and position of the i_{th} particle are updated in k_{th} iteration as follows

$$v_i(k+1) = \omega v_i(k) + c_1 r_1\big(p_i(k) - x_i(k)\big) + c_2 r_2\big(p_k(k) - x_i(k)\big) x_i(k+1) = x_i(k) \quad (17)$$

where k is the iteration times, ω is the weight of inertia, and c_1 and c_2 are acceleration factors, which control individual information feedback and group information communication of the particles, and causes the particles approach the potential optimal position through judgments based on the information from individual and group optimization and adjustment of the position. r_1 and r_2 are random numbers between 0 and 1, which improves the fault tolerance and optimization ability of the particles.

Analysis of PSO-based Automatic History Matching Results

Numerical Fitting of Experimental Data. The relative permeability curve and capillary curve were calculated by controlling points of the relative permeability curve. The value of parameters is listed in Table 3.

The PSO algorithm was used to perform history matching for 3,000 times to obtain the recovery degree, injection pressure, water cut and gas-oil ratio of cores from the low-permeability reservoir. The results are shown in **Figure 5**, and the error is less than 2%.

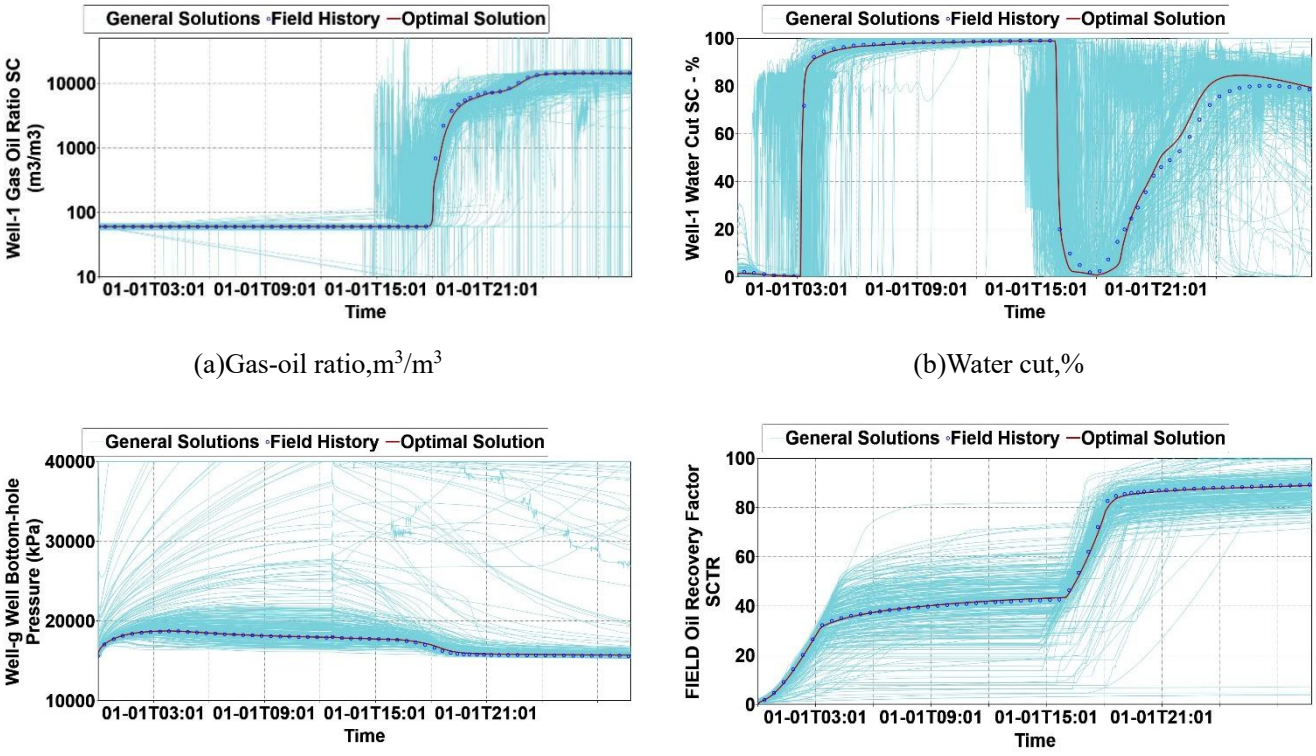

(a)Gas-oil ratio,m^3/m^3 (b)Water cut,%

(c)Injection well bottom-hole pressure, kPa (d)Oil recovery,%

Figure 5—Fitting of data from the flooding experiment of the low-permeability cores.

The variation of the global error of historical matching with the test trial is shown in **Figure 6**. It shows that the model error is less than 3% after 500 trials, but more trials are required to reduce the error. The distribution of model parameters optimized with the PSO algorithm in 3000 times is shown in **Figure 7**.

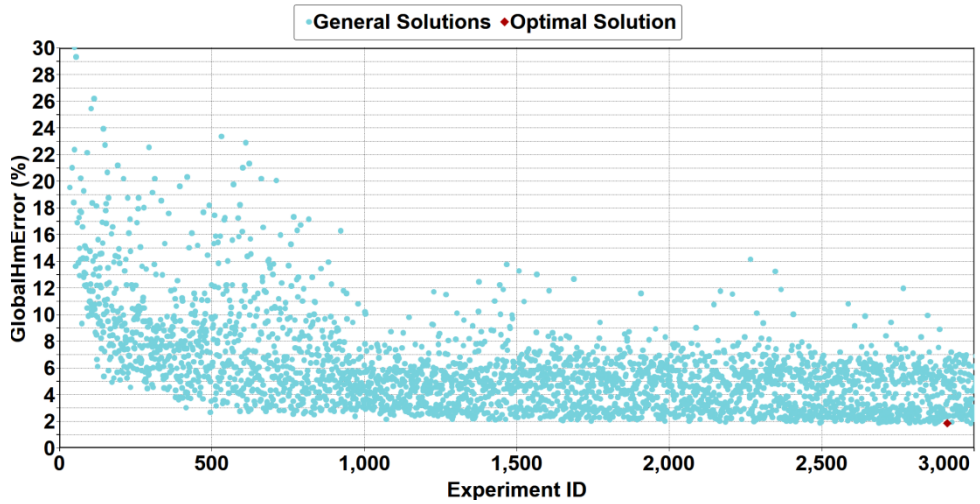

Figure 6—Global error of historical matching vs the trial number.

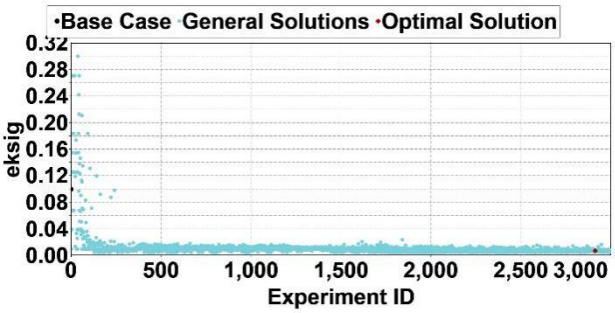

(a)eksig

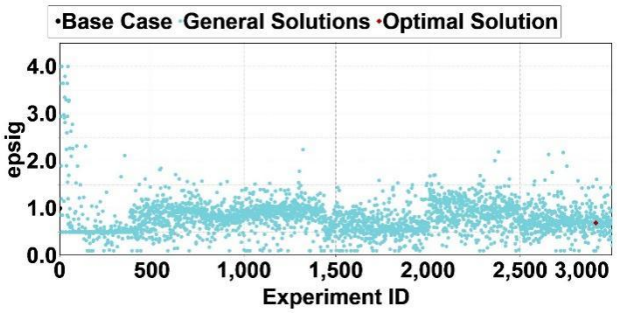

(b)epsig

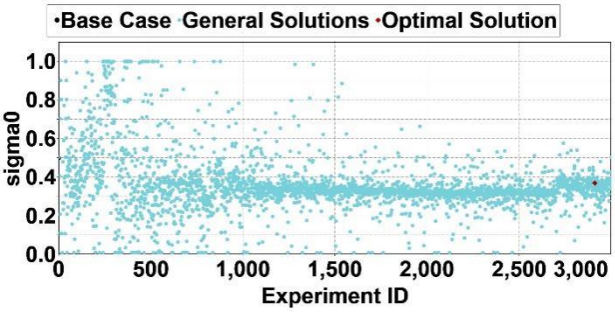

(c) σ_0

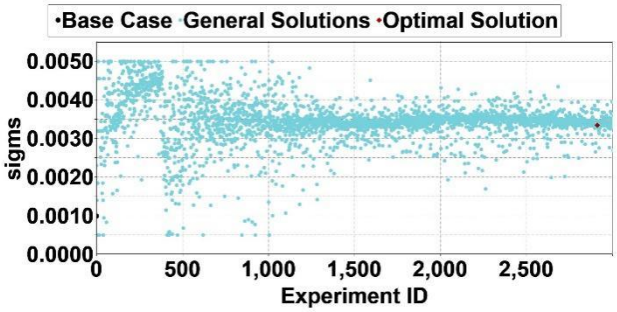

(d)sigms

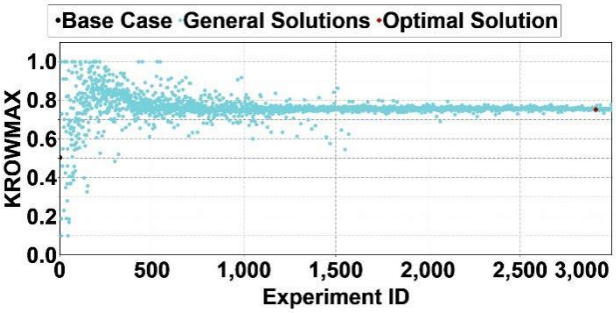

(e)KROWMAX

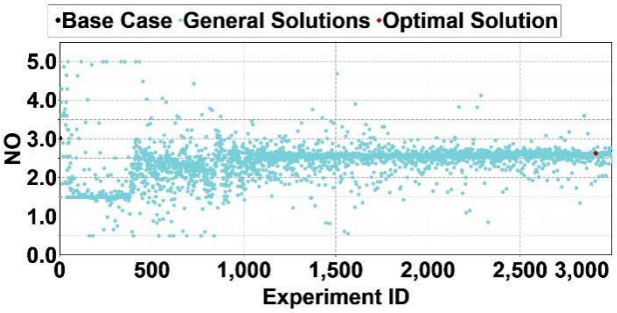

(f)NO

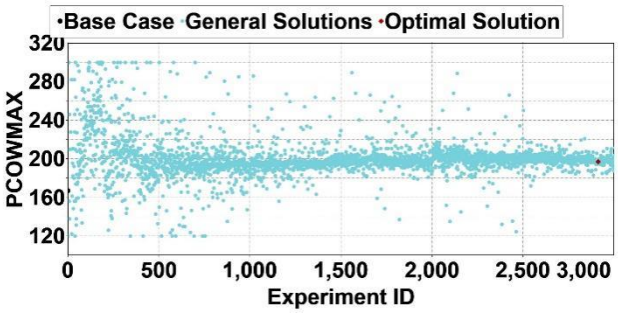

(g)PCOWMAX

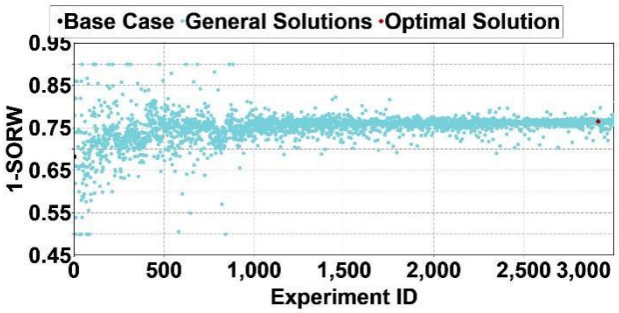

(h)1-SORW

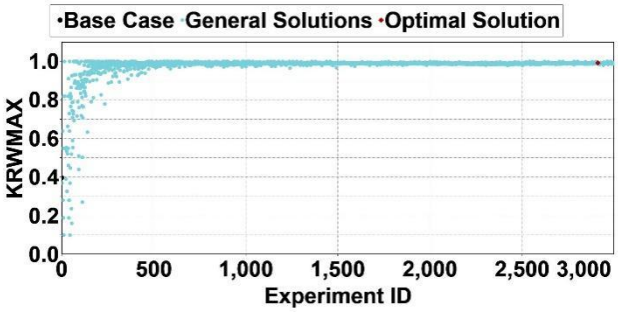

(i)KRWMAX

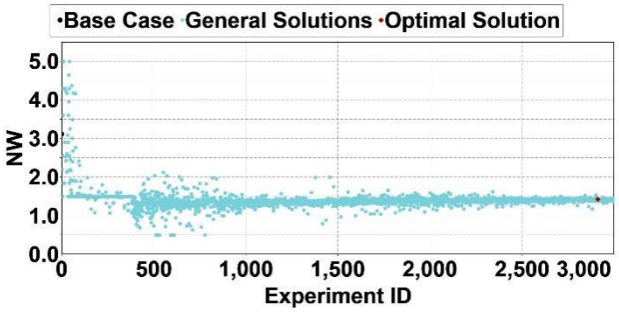

(j)NW

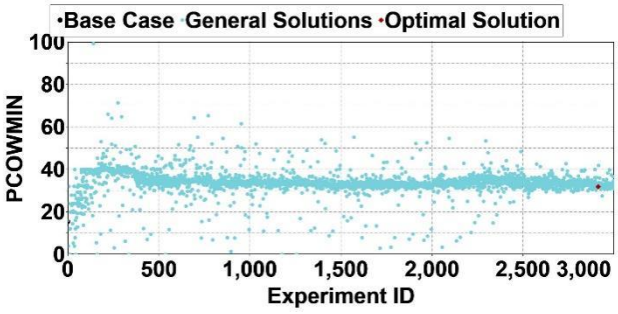

(k)PCOWMIN

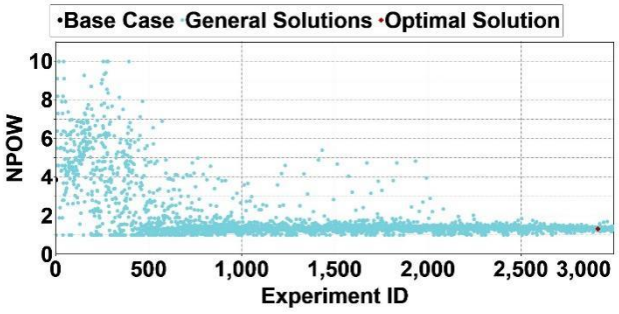

(l)NPOW

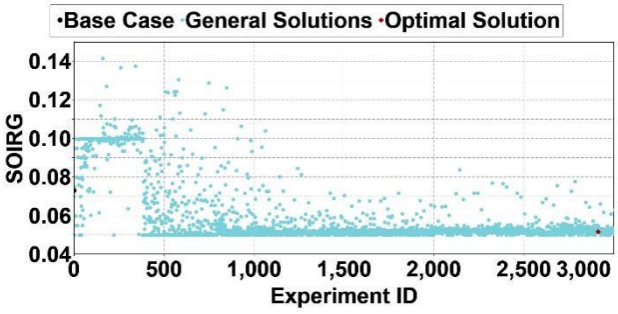

(m)SOIRG

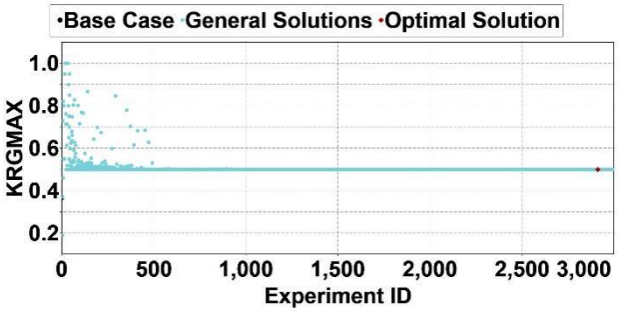

(n)KRGMAX

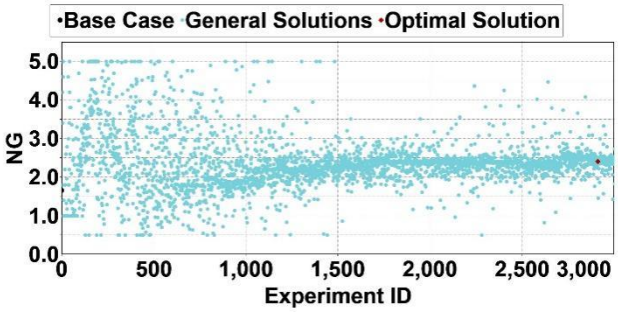

(o)NG

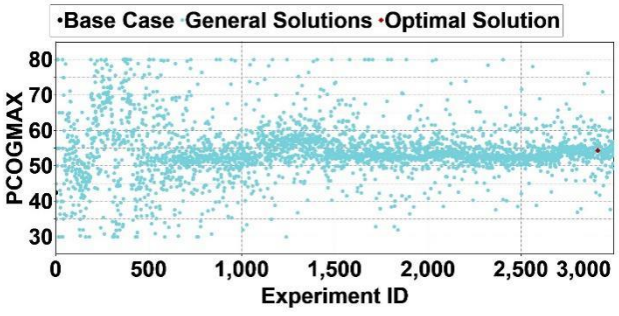

(p)PCOGMAX

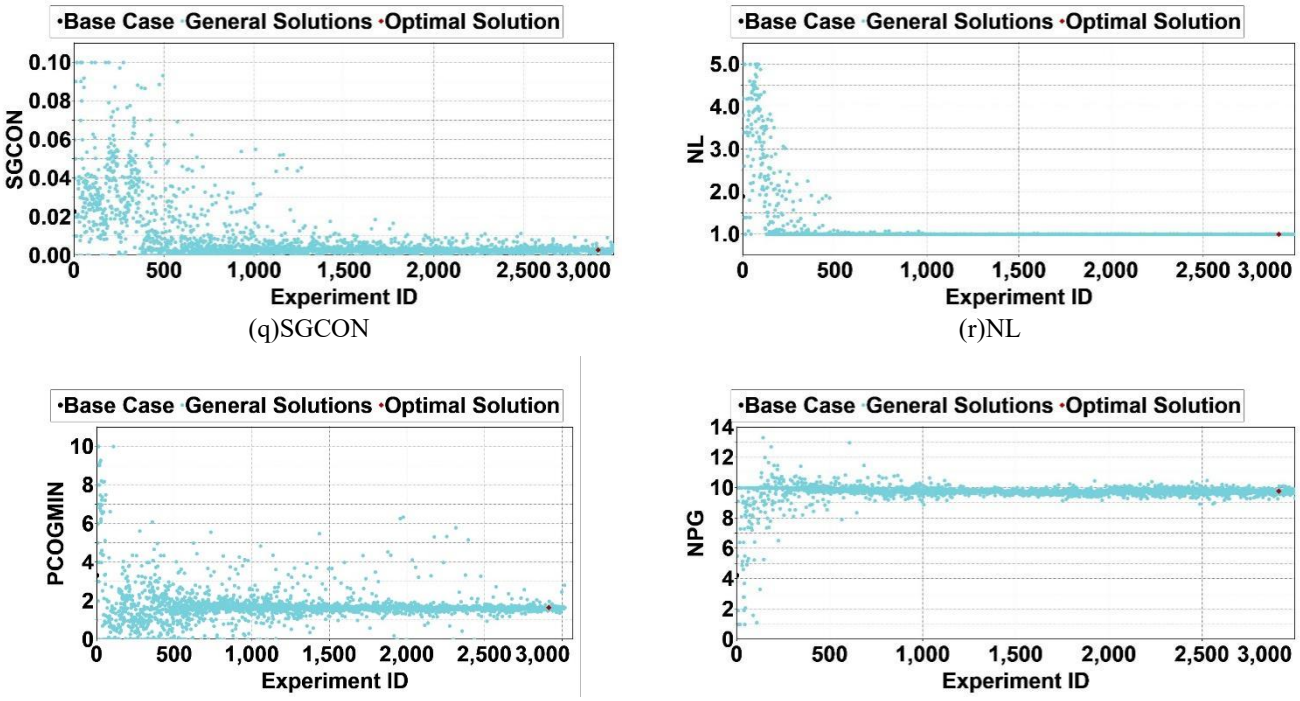

Figure 7—Distribution of parameters 3000 times during optimization.

A total of 51 cases of historical matching with an error of less than 2% were selected, and the distribution of the model parameter in the optimization of PSO is shown in **Figure 8**. It can be seen that the parameter uncertainty has been searched to a range small enough with the PSO optimization.

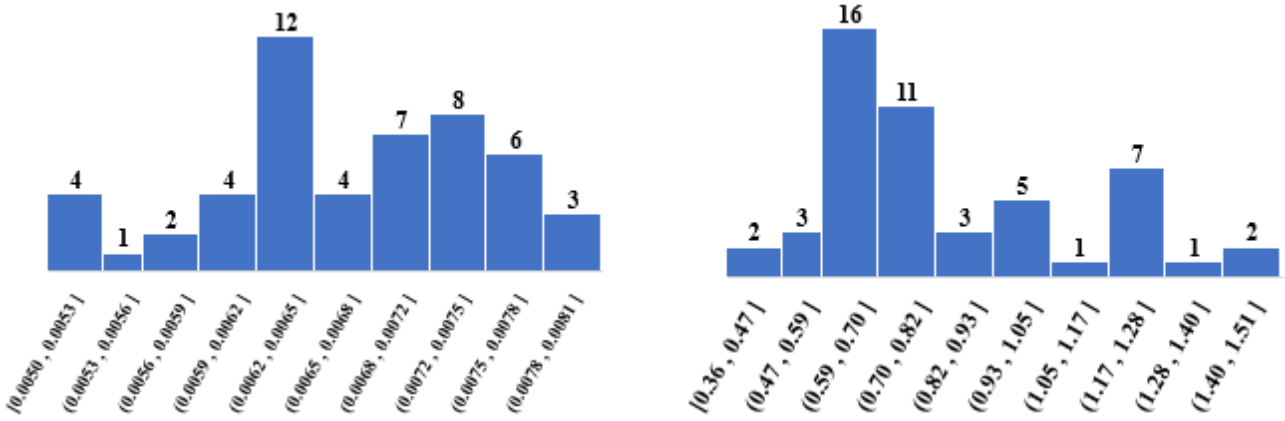

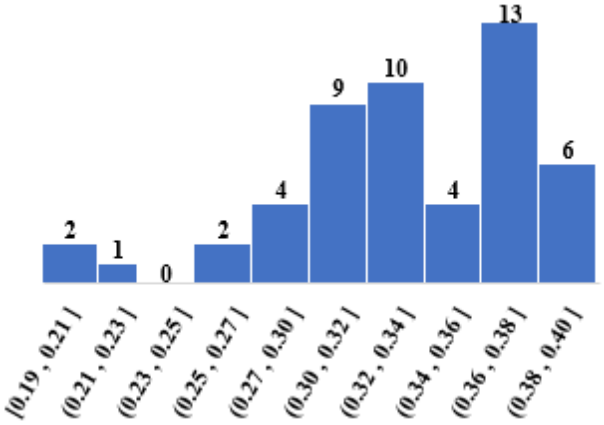

(c) σ_0

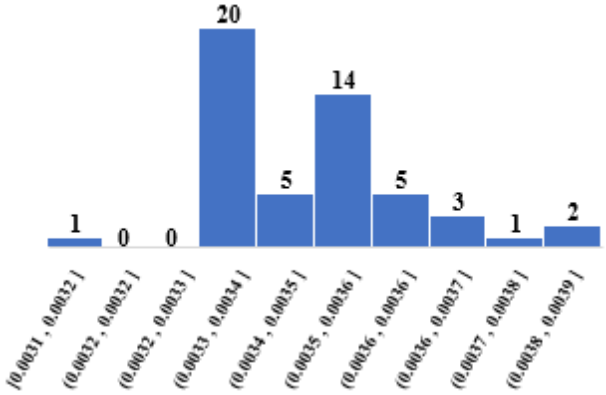

(d)sigms

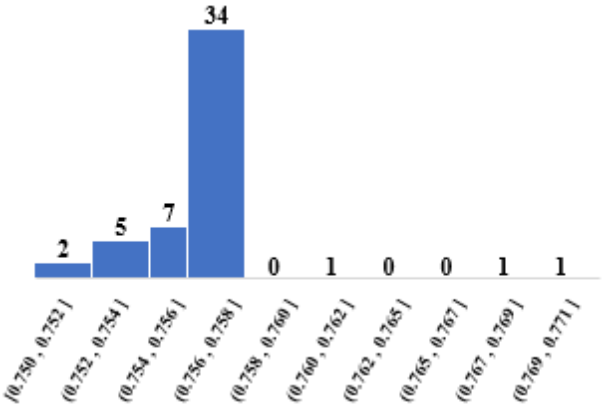

(e)KROWMAX

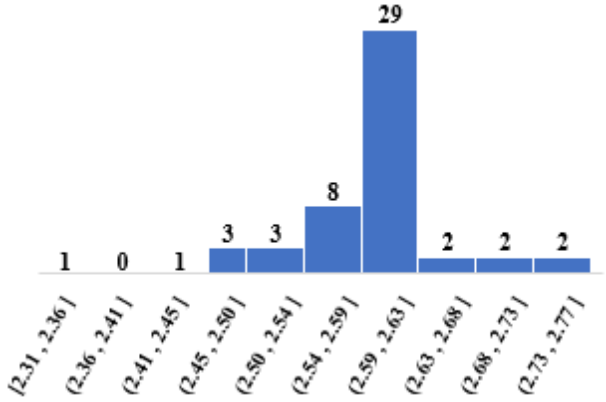

(f)NO

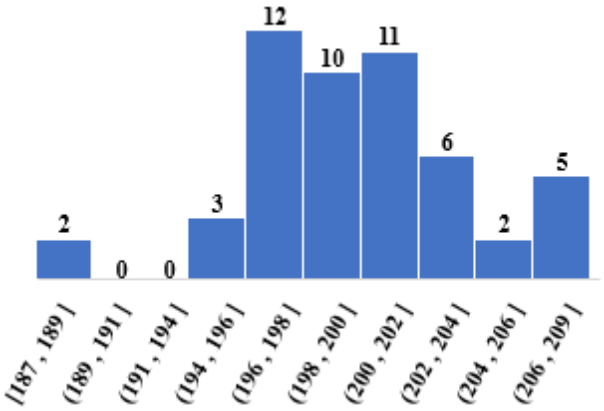

(g)PCOWMAX

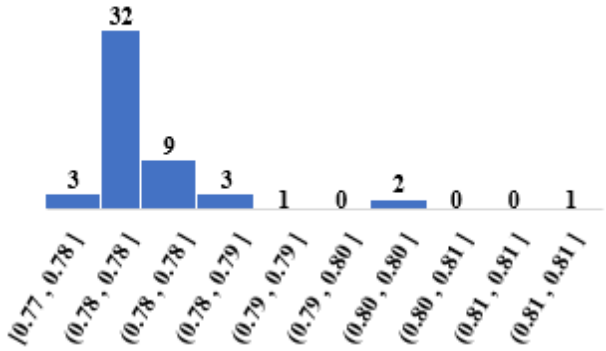

(h)1-SORW

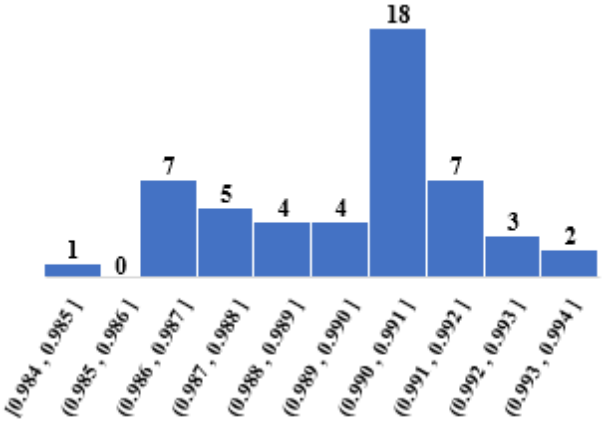

(i)KRWMAX

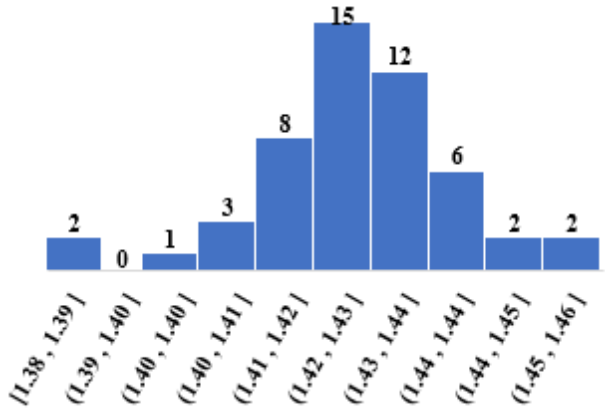

(j)NW

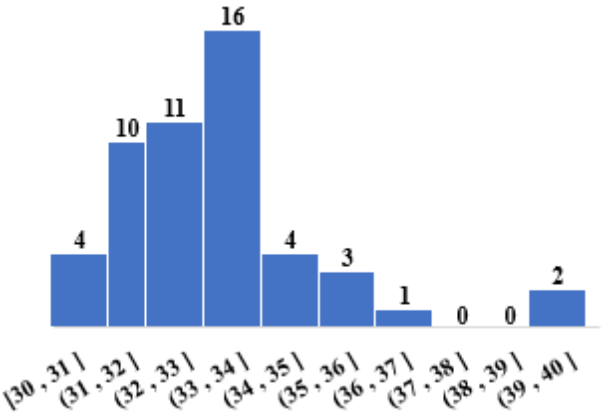

(k)PCOWMIN

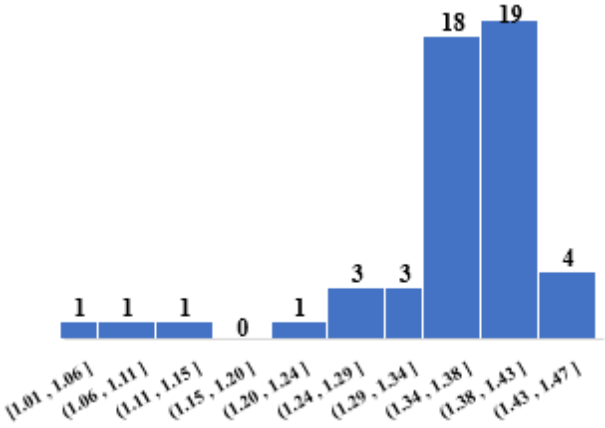

(l)NPOW

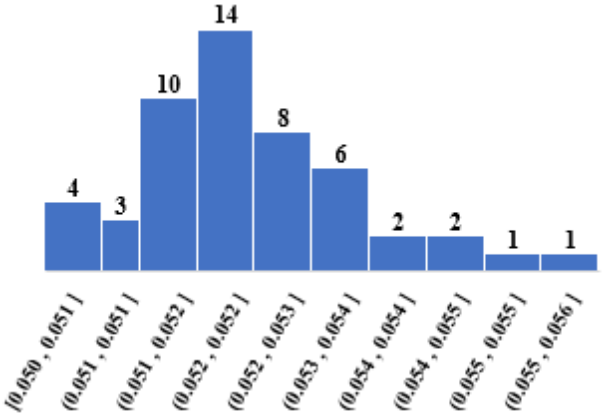

(m)SOIRG

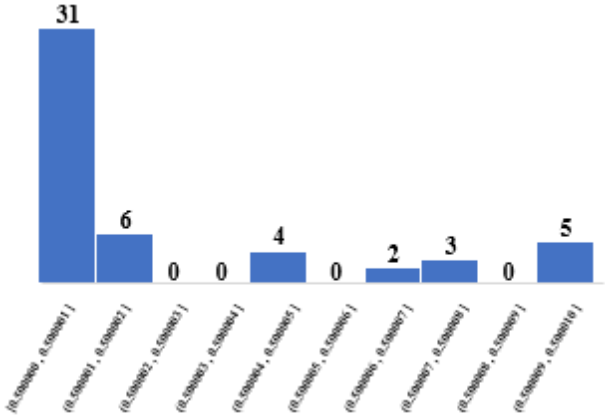

(n)KRGMAX

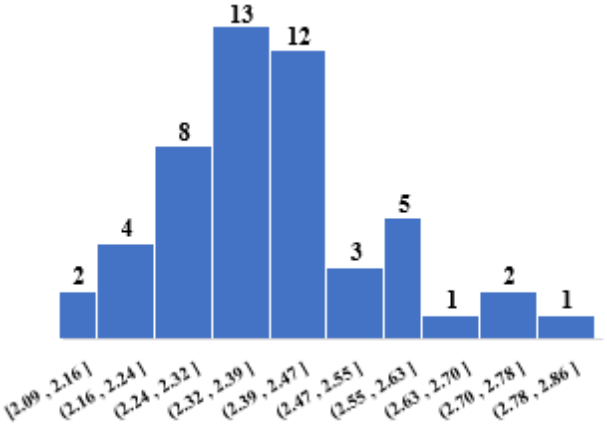

(o)NG

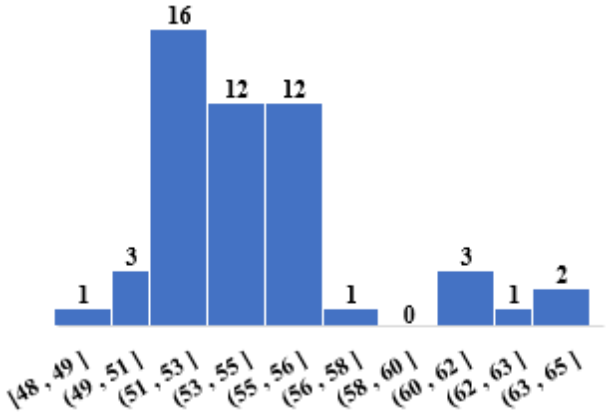

(p)PCOGMAX

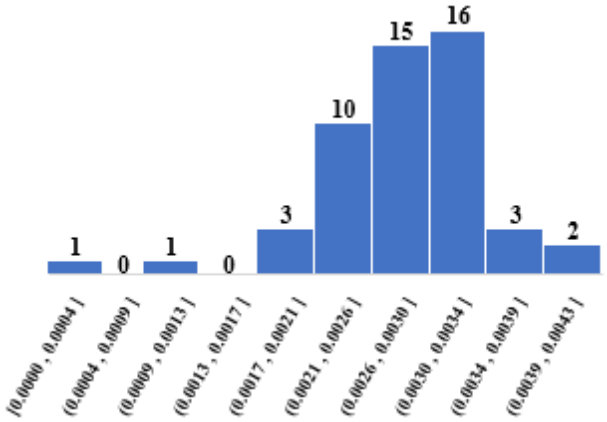

(q)SGCON

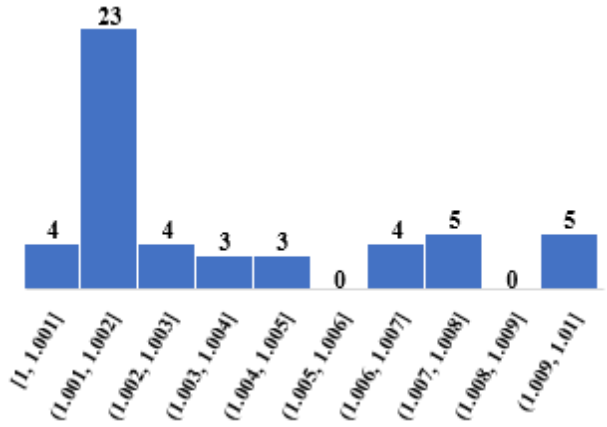

(r)NL

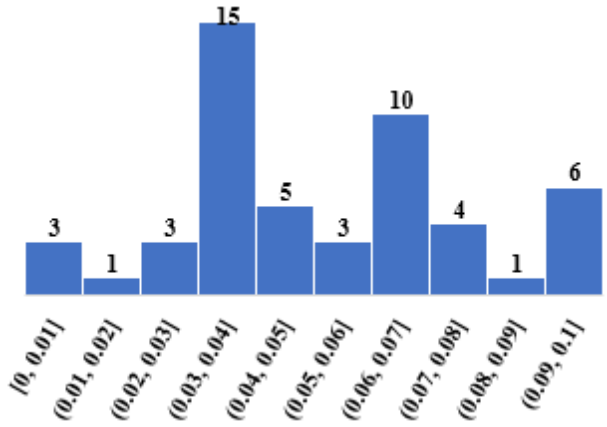

(s)PCOGMIN

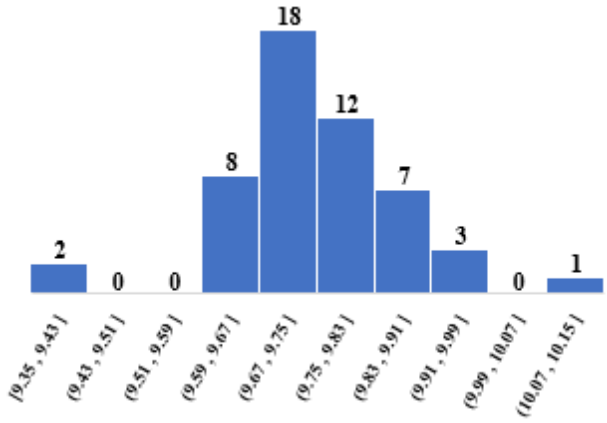

(t)NPG

Figure 8—Distribution of 51 groups of model parameters with an error of less than 2%.

Analysis of Relative Permeability Curve Characteristics. The capillary curves (**Figure 9**) and the relative permeability curves (**Figure 10**) of the low permeability reservoir cores were obtained by normalization of the capillary curves and the relative permeability curves from 51 cases of history matching with an error of less than 2%, and the characteristics of the curve endpoints are illustrated in **Table 4**. As shown in Figure 9a, the oil-water capillary pressure of low-permeability reservoirs is low, ranging from 0 to 3 MPa, and the gas-liquid capillary pressure is even lower, ranging from 0 to 0.2 MPa (Figure 9b).

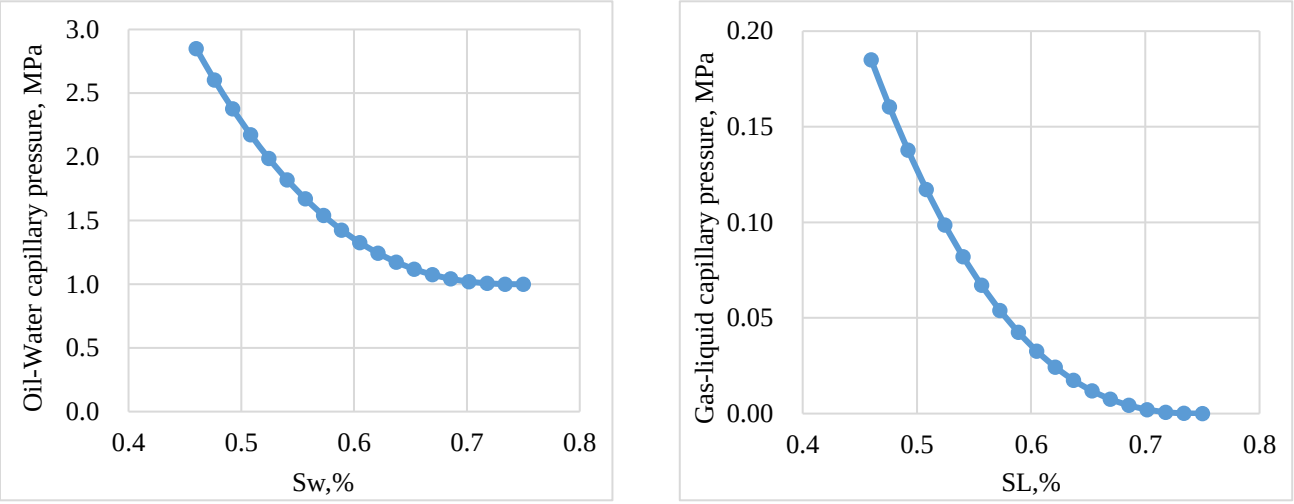

(a)Oil-water (b)Gas-liquid

Figure 9—Capillary curve of low-permeability cores.

The characteristics of the relative permeability curves are summarized as follows.

Oil-water relative permeability curve:

(1) The water saturation at the same permeability point of the oil-water relative permeability curve is 56.2%, which is greater than 50%, indicating that the reservoirs in the study area are hydrophilic.

(2) The oil-water relative permeability curve shows obvious characteristics of the displacement of water by oil in low-permeability reservoirs. The irreducible water saturation of the cores exceeds 30%, while the residual oil saturation exceeds 20%, and the range of common permeability is 33%.

(3) As water saturation increases, the relative permeability of the oil decreases rapidly and the relative permeability of the water increases.

Gas-liquid relative permeability curve:

(1) The irreducible liquid saturation exceeds 30%, and the residual gas saturation is 11%.

(2) As the gas saturation increases, the relative permeability of the liquid decreases significantly, and the relative permeability of the gas increases significantly, indicating that the oil flow is affected both by gas and liquid.

(3) The gas-liquid common permeability range is 54%. The common permeability range of oil and gas is larger than that of oil and water, which is conducive to more oil displacement. This indicates that compared to the development of water flooding, CO_2 injection is more conducive to improving oil recovery of this type of reservoir and increases oil recovery by more than 10%.

Table 4—Relative permeability of low permeability reservoirs.

Oil-water	Permeability (mD)	Porosity (%)	S_{wcon} (%)	S_{orw} (%)	k_{rwiro} (%)	S_w @ isosmotic point (%)	Two-phase flow region (%)
	1.2	13.2	35	32	18	56.2	33.0
Gas-liquid	Permeability (mD)	Porosity (%)	S_{lcon} (%)	S_{gcrit} (%)	k_{rgcl} (%)	S_l @ isosmotic point (%)	Two-phase flow region(%)
	1.2	13.2	35	11	42.4	60.1	54.0

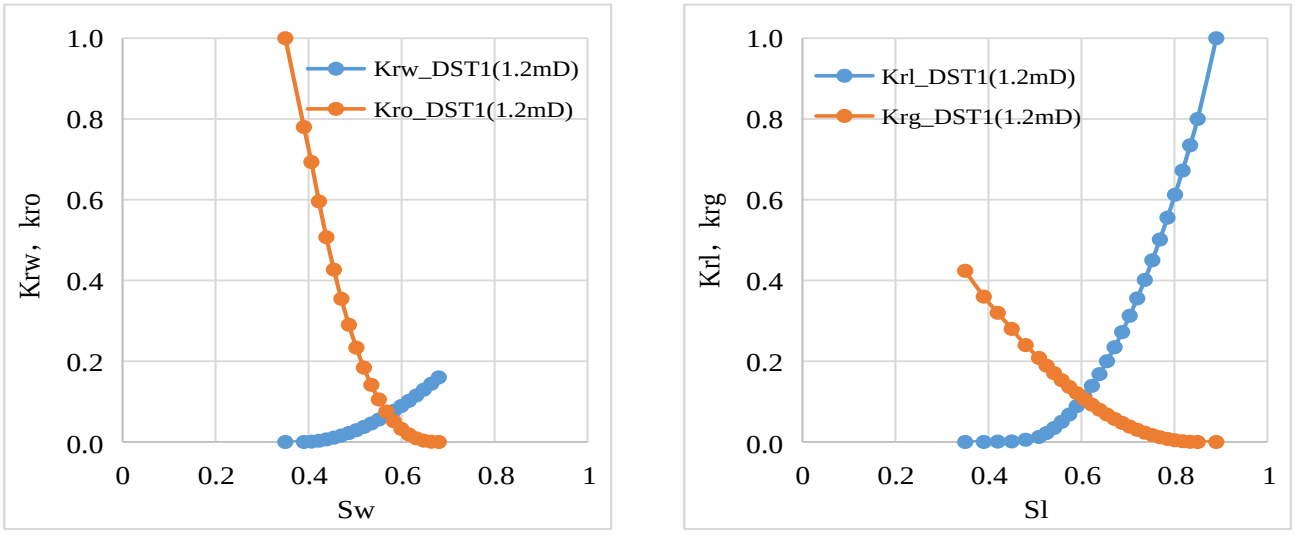

(a)Oil-water (b)Gas-liquid

Figure 10—Relative permeability curve of low permeability cores.

Conclusions

In this paper, a PSO-based method of fitting the relative permeability was proposed. The CO_2 flooding experiments in long cores from low-permeability reservoirs were performed to obtain flow and pressure data. The Corey model was used to characterize the permeability curve, where the permeability and capillary pressure models include 26 parameters. The core experimental data were fitted by adjusting the Corey model and the capillary curve with the PSO method, and the fitting error is less than 2%. The relative permeability curve and the capillary curve of the experimental core were obtained. The curve characteristics are as follows.

1. The water saturation at the same permeability point of the oil-water relative permeability curve is 56.2%, which is higher than 50%, indicating that the reservoirs in the study area are hydrophilic. The oil-water relative permeability curve shows obvious characteristics of the displacement of water by oil in low-permeability reservoirs.
2. The common permeability range of oil and gas is larger than that of oil and water, which is conducive to more oil displacement. This indicates that compared to the development of water flooding, CO_2 injection is more conducive to improving the oil recovery of this type of reservoir.
3. The oil-water capillary pressure of low-permeability reservoirs is low, ranging from 0 to 3 MPa, and the gas-liquid capillary pressure is even lower, ranging from 0 to 0.2 MPa.

Nomenclature

k_{rg}	=	relative permeability of gas
k_{rgcl}	=	krg at connate liquid saturation
k_{rw}	=	relative permeability of water
k_{rwiro}	=	krw at irreducible oil saturation
k_{row}	=	krw in the presence of the given water saturation
k_{rocw}	=	krw at connate water saturation
k_{rog}	=	krw in the presence of the given water saturation
k_{rogcg}	=	krog at connate gas saturation
n_g	=	exponent for calculating krg
n_w	=	exponent for calculating krw

n_{ow} = exponent for calculating krow

n_{og} = exponent for calculating krog

S_{gcon} = connate gas saturation

S_{gcrit} = critical gas saturation

S_l = liquid saturation

S_{lcon} = irreducible liquid saturation, Swcon+Soirg

S_o = oil saturation

S_{org} = residual oil saturation for gas-liquid table

S_{orig} = non-reducible oil saturation for oil-gas table

S_{oirw} = non-reducible oil saturation for oil-water table

S_{orw} = residual oil saturation for oil-water table

S_w = water saturation

S_{wcrit} = critical water saturation

S_{wcon} = connate water saturation

p_{cow} = oil-water capillary pressure

p_{cog} = gas-liquid capillary pressure

SWCON = connate water saturation

SWCRIT = critical water saturation

SORW = residual oil saturation

SOIRW = irreducible oil saturation for oil-water table

KROWMAX = maximum krow

KRWMAX = maximum krw

NO = exponent for calculating krow from krocw

NW = exponent for calculating krw from krwiro

SOIRG = irreducible oil saturation for gas-liquid table

SORG = residual oil saturation for gas-liquid table

SGCON = connate gas saturation

SGCRIT = critical gas saturation

KRGMAX = maximum krg

KROGMAX = maximum krog

NG = exponent for calculating krog from krogcg

NL = exponent for calculating krg from krgcl

PCOWMAX = maximum oil-water capillary pressure

PCOGMAX = maximum oil-gas capillary pressure

PCOWMIN = minimum oil-water capillary pressure

PCOGMIN = minimum oil-gas capillary pressure

NPOW = exponent for calculating oil-water capillary pressure

NPGL = exponent for calculating gas-liquid capillary pressure

Greek letters

σ = oil-gas interfacial tension calculated through the MacLeod-Sugden correlation

σ_0 = referenced interfacial tension when calculating the relative permeability

eksig = gas-oil relative permeability index (dimensionless)

epsig = gas capillary pressure index (dimensionless)

Acknowledgements

The authors are grateful for financial support from the National Science and Technology Major Project (Grant No. 2016ZX05016-005 and 2016ZX05016-001), the Major Project of China National Petroleum Corporation (Grant No. RIPED-2020-JS-50214) and (Grant No. RIPED-2020-JS-50215), the project of Sinopec North China Petroleum Bureau (Grant No. 290018276) and project of Petroleum Engineering Technology Institute of SINOPEC Shengli Oilfield (Grant No. 290018276).

Conflicts of Interest

The author(s) declare that they have no conflicting interests.

References

CMG Manual 2015. Computer Modeling Group.

Eydinov, D., Gao, G., Li, G., et al. 2009. Simultaneous Estimation of Relative Permeability and Porosity/Permeability Fields by History Matching Production Data. *Journal of Canadian Petroleum Technology* **48**(12):13-25.

Li, K.1989. An Optimization Method for Calculating the Relative Permeability Curve of Oil And Water Based on the Experimental Data of Dynamic Displacement. *Journal of Oil and Gas Technology* **11**(3) :45-54.

Li, Y., Li, Y., Yu, L., et al. 2018. Review of History Matching Method for Calculating Oil-Water Relative Permeability Curves. *Journal of Longdong University* **29**(3):55-58.

Toth, J., Tibor, B., Peter, S., et al. 2002. Convenient Formulae for Determination of Relative Permeability from Unsteady-State Fluid Displacements in Core Plugs. *Journal of Petroleum Science and Engineering* **36**(1):33-44.

Zhang, F., Wang, Z., Cheng, Y., et al. 2010. Processing Methods for Relative-permeability Curves in Reservoir Numerical Simulation. *Natural Gas Geoscience* **21**(5):859-862.

Zhang, Q. 2017. Research on the Particle Swarm Optimization and Differential Evolution Algorithms. PhD dissertation, Shandong University, Jinan, China.

Zhang, X., Du, J., Bai, L., et al. 2016. New Calibration Method for Oil-Water Relative Permeability Curves Based on Unsteady State Method. *Fault-Block Oil & Gas Field* **23**(2):185-188.

Zhang, Z., Tong, Y., and Wu, Y. 2019. Effects of Diffusion on Relative Permeability Curves of CO_2 Flooding in Low Permeability Reservoirs. *Journal of Xi'an Shiyou University (Natural Science Edition)* **34**(2):73-77.

Weiling Zhang is a engineer in Tianjin Branch of CNOOC. His research interests include numerical simulation and field development of offshore reservoirs.

Wenfeng Lv is a senior engineer at the Research Institute of Petroleum Exploration and Development (RIPED), PetroChina. He holds a PhD degree from China University of Petroleum. His research interest includes numerical simulation and gas flooding.

Yongyi Zhou, North China Petroleum Bureau, Sinopec. His research interest includes numerical simulation and field development for unconventional reservoirs.

Bochao Qu is a master candidate in Petroleum Engineering Department at Xi'an Shiyou University. His research interests include reservoir simulation and production analysis.

Yawen He is a master candidate in Petroleum Engineering Department at Xi'an Shiyou University. Her research interests include reservoir simulation and hydraulic fracturing design.

Xinle Ma is a master candidate in Petroleum Engineering Department at Xi'an Shiyou University. Her research interests include big data, reservoir simulation, and production analysis.

Weidong Tian is a master candidate in the Department of Petroleum Engineering at Xi'an Shiyou University. He has focused his research in areas involving reservoir simulation, well testing and production analysis.

Zhenzhen Dong is a Professor in the Department of Petroleum Engineering at Xi'an Shiyou University. She worked as a reservoir engineer at Schlumberger from 2012 to 2016. Her research interests include unconventional resources/reserves estimates, reservoir simulation, well testing, and production analysis. Dr. Dong holds a bachelor's degree in Mathematics from Northeast Petroleum University, China; a master's degree in Petroleum Engineering from Research Institute of Petroleum Exploration and Development (RIPED), China; and a PhD degree in Petroleum Engineering from Texas A&M University.